Pseudoprospective forecasting of failure time

Shengwang Hao,[1,2,*] Peng Cui,[1] Sunji Zhou,[1] Liwei Wang,[1,2] and Derek Elsworth[3]

[1]*School of Civil Engineering and Mechanics, Yanshan University, Qinhuangdao 066004, China*

[2]*Hebei Key Laboratory of Green Construction and Intelligent Maintenance for Civil Engineering, Hebei Province Engineering Research Center for Harmless Synergistic Treatment and Recycling of Municipal Solid Waste, Yanshan University, Qinhuangdao 066004, China*

[3]*Energy and Mineral Engineering, Geosciences, G3 Center, and EMS Energy Institute, Pennsylvania State University, University Park, Pennsylvania, USA*

(Received 5 March 2025; accepted 5 May 2025; published 5 June 2025)

Power-law precursory acceleration of observable quantities has been accepted as an effective way to predict time to failure in both materials and structures. However, the form of the power-law exponent is seldom known *a priori* and is a key challenge in blind prediction. We report a linear relation with respect to time t of the estimated failure times t_* that are calculated step by step using the most recent updates of the monitored quantity. Our findings indicate that the monitored quantity can be defined as any power of the inverse rate. All projections of t_* for any exponent universally intersect with the straight line of $t = t_*$, with the intersection uniquely defining the failure time. The method is validated against synthetic data, laboratory experiments (materials failure), and volcanic eruption data (structural failure). Our work provides the basis for a significant improvement in time to failure forecasting where the controlling power-law exponent is not known in advance.

DOI: 10.1103/PhysRevE.111.065503

I. INTRODUCTION

The increase in acceleration of measurable quantities such as deformation or (micro)seismicity preceding the time of failure of materials and structures is widely observed and accepted as a proxy for a precursor to failure [1–9]. In the vicinity of the failure time t_f, this acceleration precursor can be described as a power-law relation [1–3,7–14]

$$\dot{\Omega} = C(t_f - t)^{-\beta} \tag{1}$$

with respect to the time to failure, where Ω represents a measurable quantity and the overscripted dot represents the derivative of Ω with respect to time. β is the critical power-law exponent and C is a prefactor. Equation (1) can be deduced from Voight's relation [1,2,7–11]

$$\dot{\Omega}^{-\alpha}\ddot{\Omega} - A = 0 \tag{2}$$

that describes the behavior of materials in their terminal stage of failure, with $C = [A(\alpha-1)]^{1/(1-\alpha)}$ and $\beta = 1/(\alpha-1)$ [1], where A and α are constants. $\dot{\Omega}$ tends to infinity as time approaches the failure time. This power-law behavior has been confirmed by observations for natural hazards such as landslides [14,15], volcanic eruption [1–3,5,9], and failure in laboratory experiments [16–23].

Equation (1) can be rewritten in a linearized form [10,11,23]

$$\dot{\Omega}^{-1/\beta} = C^{-1/\beta}(t_f - t). \tag{3}$$

Then the failure time can be determined by linearly extrapolating the curve of $\dot{\Omega}^{-1/\beta}$ with time to its intersection with the time axis. This failure forecast method (FFM) [9,10,16,24,25] has been proven of validity in the retrospective prediction of failure in laboratory experiments [17,20], landslides [4,26], volcanic eruptions [1,3–5,27–29], and structural health monitoring [30]. Many attempts have been made to assess and improve the accuracy of this method for forecasting failure [13,21,30–34] in real time.

The common application of the FFM always supposes that the exponent β is unity ($\beta = 1$), i.e., $\alpha = 2$. In this case, the inverse rate decreases linearly with time. However, laboratory experiments and field data show that the exponent β does not always take the value of unity. Thus in the application of blind prediction for failure in real time, a key difficulty is that the actual value of β (α) is in fact unknown and shows a large dispersion immediately prior to failure [2,3,5,11,13,23,25].

We report a method that is unencumbered by this *apriori* uncertainty of the exponent β (α) for blind prediction in real time. In this method, we first calculate the values of any power χ of the inverse rate. Then a sequence of estimated values t_* of the failure time can be determined by fitting the recent data to Eq. (3) step by step. Our findings indicate that the estimated values t_* consistently converge to the actual failure time as a linear tendency with respect to time. These evolving lines of t_* estimated by different values of χ have a common intersection point at $t_* = t = t_f$ with the line of $t = t_*$. Consequently, the failure time can be predicted as the intersection point in real time. These results are confirmed by synthetic data, laboratory experiments, and volcanic eruption data.

II. PREDICTIONS THROUGH THE CLASSIC FFM

For the classic FFM [1–6,9–11,17,24], the exponent β is assumed to be equal to 1 and the failure time is estimated

*Contact author: hsw@ysu.edu.cn

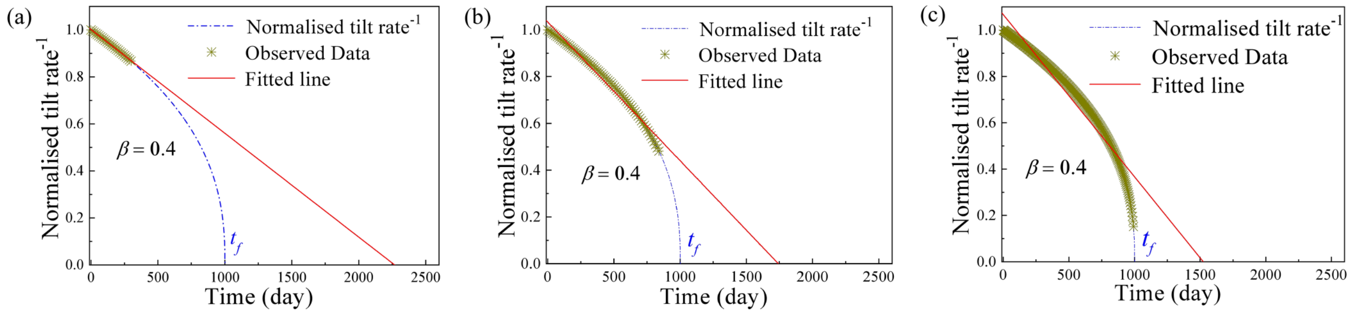

FIG. 1. Key difficulties and errors in the prediction process using the cumulative-time technique. Every fit of the data begins from the same initial time but ends at every individual current time. Consequently, the number of data points used in fitting increase as time approaches the failure time. The solid red lines are the fitted results and the intersection point with time axis is the predicted result.

by extending the inverse rate to intersect the time axis. Two estimation methods named, respectively, the "cumulative" and "simple moving-time window" techniques [11] can be used to perform the prediction. For the "cumulative-time technique" (Fig. 1), every fitting starts from the same initial time but ends at every individual observation time. For the "simple moving-time window technique" (Fig. 2), only the most recent data (within a window) are used and thus the start time varies as the window moves. This process is equivalent to fitting the tangent to the function at every individual update with the failure time identified at the intersection of this projected tangent with the time axis. In both techniques, the linear fitting is made stepwise, with the observation time progressing towards the failure time.

It is apparent that the FFM method produces a biased prediction, leading to significant errors when β is not close to 1, especially at the earliest stages (Figs. 1 and 2). The failure times are overestimated when $\beta < 1$ (Figs. 1 and 2) since the curve of the inverse rate is upwardly convex. Conversely, when $\beta > 1$ the failure times are underestimated. Only when the observation time is very close to the failure time will predictions converge to the true failure time. Considering the properties of the change in the gradient of the inverse rate over time, in practical application, the "simple moving-time window" technique is preferred since the previous data have little effect on the current prediction and the prediction converges more rapidly to the actual value. Thus, understanding the tendency of the predicted values t_* to converge to the true failure time could present an earlier and more accurate blind prediction when β is unknown.

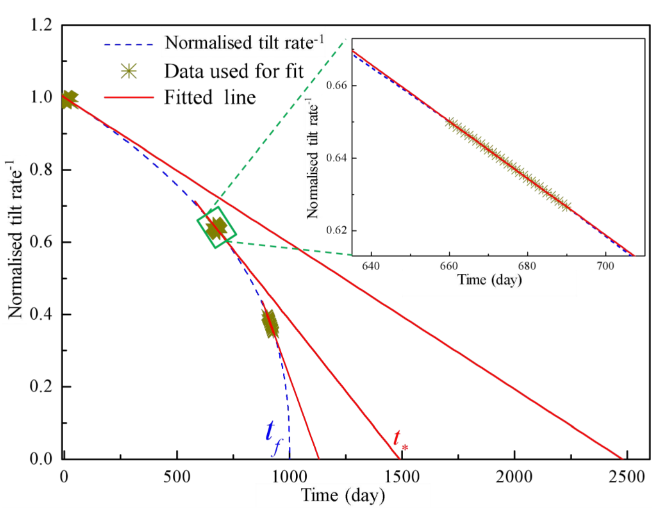

FIG. 2. Key difficulties and errors in the prediction process in applying the simple moving-time window technique. During the process of fitting, only the most recent data (within a window) are used in the prediction, i.e., the starting and ending time of the data points used for the prediction vary as the window moves. The solid red lines are the fitted results and the intersection point t_* with time axis is the predicted result. The inset shows a zoomed-in view to the fit result.

III. A LINEAR RELATION FOR THE BLIND PREDICTION OF FAILURE TIME

In order to reveal the general tendency of the predicted values t_* converging to the actual failure time when β is unknown, let us raise both sides of Eq. (1) to the $1/\chi$ power to get

$$\dot{\Omega}^{-1/\chi} = C^{-1/\chi}(t_f - t)^{\beta/\chi}. \tag{4}$$

Clearly, the function $\dot{\Omega}^{-1/\chi}$ versus time is upwardly convex when $\chi > \beta$, concave when $\chi < \beta$ (Fig. 3) and linear when $\chi = \beta$. In application of the classic FFM [1–6,9–11,17,24], the inverse rate is used to perform the prediction. This is equivalent to setting $\chi = 1$.

Straightforwardly, the equation of the tangent to the function $\dot{\Omega}^{-1/\chi}$ versus time at any point $(t, \dot{\Omega}^{-1/\chi})$ can be defined as

$$\dot{\Omega}^{-1/\chi} = b + kt, \tag{5}$$

where k is the slope of the tangent at time t that can be calculated as

$$k = -\frac{\beta}{\chi}C^{-1/\chi}\ (t_f - t)^{\beta/\chi - 1} \tag{6}$$

by the differentiation of Eq. (4) with respect to time. This defines the parameter b as

$$b = C^{-1/\chi}\ (t_f - t)^{\beta/\chi} - kt. \tag{7}$$

By substituting $\dot{\Omega}_f^{-1} = 0$ at the failure time into Eq. (5), the estimated failure time t_* is then calculated from

$$t_* = -b/k. \tag{8}$$

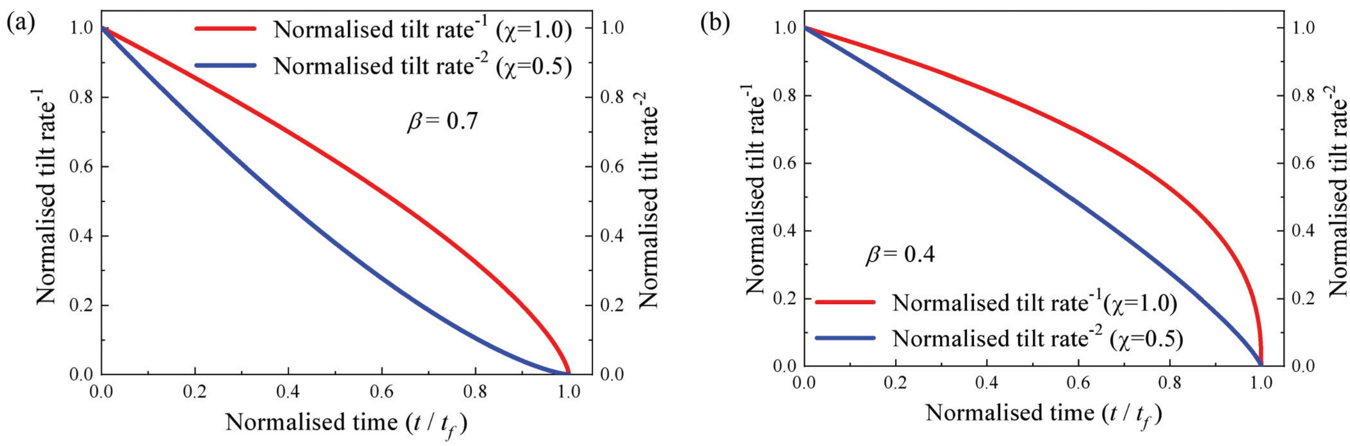

FIG. 3. Two examples illustrate the evolution of $\dot{\Omega}^{-1/\chi}$ versus time with $\chi = 1.0$ (inverse rate) and 0.5 (square of the inverse rate). The strain rates are calculated through Eq. (1) and normalized to the rate of t_0. (a) $\beta = 0.7$, (b) $\beta = 0.4$. A small amount of Gaussian noise with standard deviation 10^{-6} is added to represent the effect of measurement errors.

Substituting Eqs. (6) and (7) into Eq. (8) produces

$$t_* = \frac{\chi}{\beta} t_f + \left(1 - \frac{\chi}{\beta}\right) t. \tag{9}$$

Thus, t_* has a linear relation with respect to t with a negative slope when $\chi > \beta$ or positive slope when $\chi < \beta$. $t_* = t_f$ in the case of $\chi = \beta$. It is clear that the extrapolated tangents to Eq. (9) for different values of χ have a common intersection

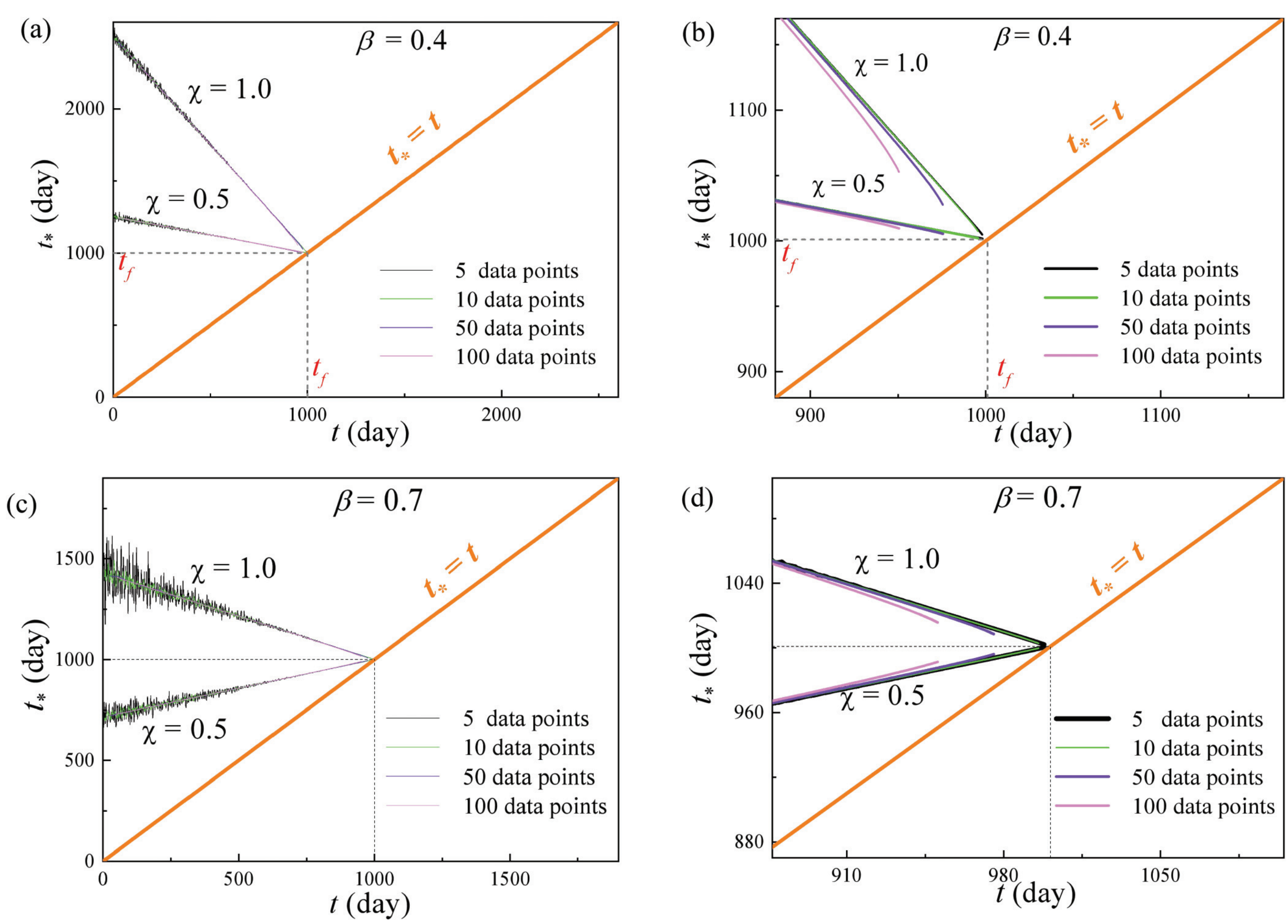

FIG. 4. Results for synthetic rates given by Eq. (1) when $\beta = 0.4$ [(a) and (b)] and $\beta = 0.7$ [(c) and (d)]. (b) and (d) are zoomed-in views of the results in the vicinity of the failure time. Four different results are calculated with 5, 10, 50, then 100 data points, respectively, used in the fit, for comparison. Three individual lines for $\chi = 1.0$, $\chi = 0.5$, and for $t_* = t$ intersect at $t = t_* = t_f$. Dashed vertical and horizontal lines denote the true failure time t_f of 1001 days.

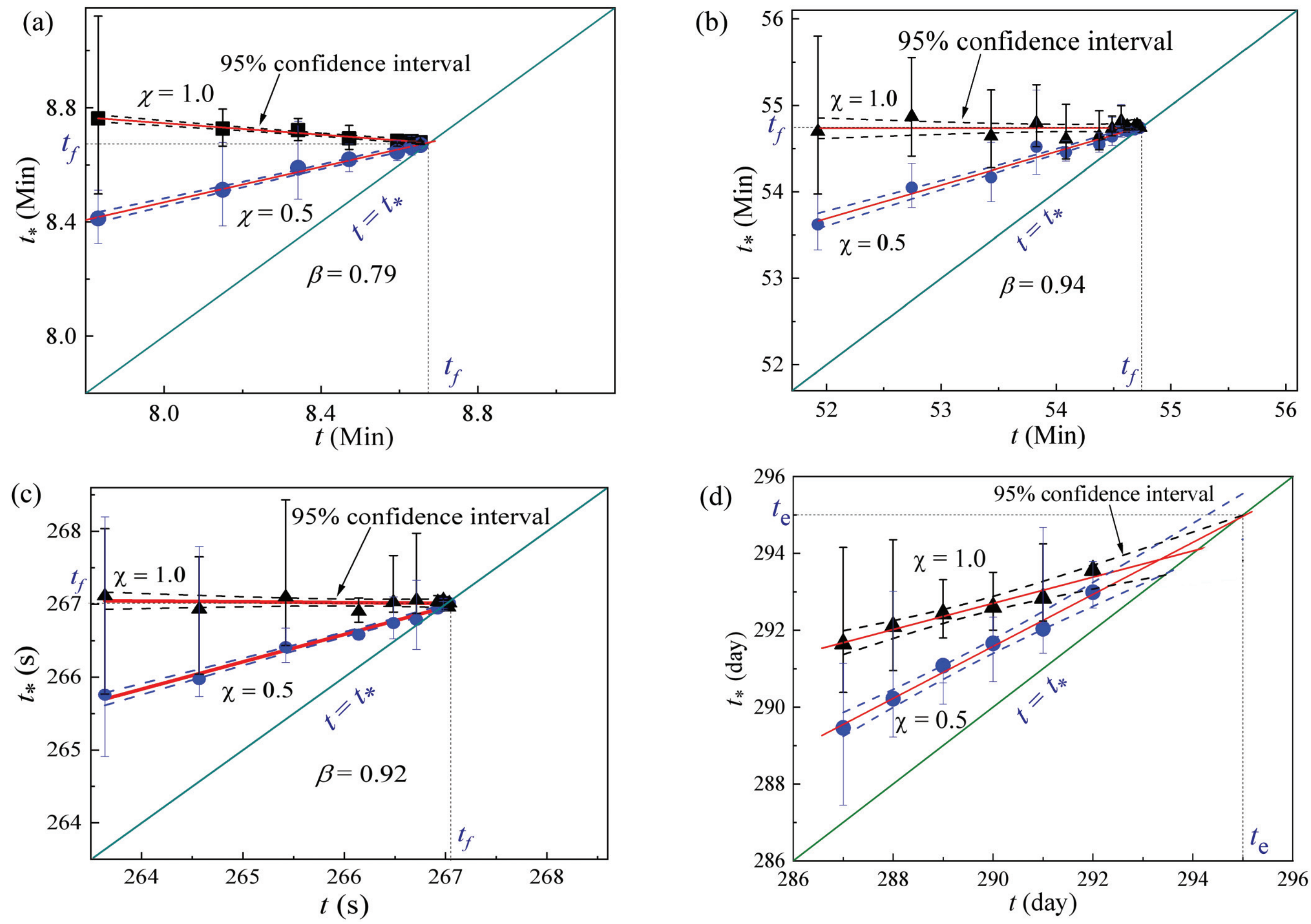

FIG. 5. Estimated failure time t_* versus time for three real data sets. Red lines are the linear fit lines. Dashed vertical and horizontal lines mark the failure time t_f, or eruption time t_e. Estimation method of error bars in t_* is illustrated in Fig. 6. (a) Creep-relaxation failure experiment, $\beta = 0.79$. (b) Creep failure experiment with $\beta = 0.94$. (c) Uniaxial compression failure experiment of volcanic basaltic rock, $\beta = 0.92$. (d) Volcanic results of one-day average tilt data [9] with $\beta = 1.84$. The first four values of t_* are through the most recent prior data points of every observable time, constituting a total of five data points, with the remaining values close to the failure time calculated through three data points. The confidence limit (especially the upper limit) is sometimes not convergent for the linear extrapolation of three data points at the 95% confidence level, because there are insufficient data points and their fluctuation is too large, and thus a 90% confidence level is selected.

point at $t = t_f$ with the line $t_* = t$. As a consequence, the failure time can be found by extending the line of Eq. (9) to the line of $t_* = t$, or determined as the intersection of two extension lines of Eq. (9) for any two values of χ.

IV. VALIDATION OF PREDICTION PERFORMANCE THROUGH SYNTHETIC AND REAL DATA

Generally, using the inverse rate $\dot{\Omega}^{-1}$ ($\chi = 1$) and the square $\dot{\Omega}^{-2}$ ($\chi = 0.5$) of the inverse rate is convenient in application. We first evaluate this method by using synthetic strain sequences where the rate evolves according to Eq. (1) with a failure time of 1001 days. Gaussian noise is added to simulate the effect of measurement errors. Figure 4 shows the results when $\beta = 0.7$ and 0.4 as two independent examples. In these cases, we do not directly calculate the derivatives of the curves of $\dot{\Omega}^{-1}$ and $\dot{\Omega}^{-2}$. Alternatively, for practical application, we use the "simple moving-time window technique" [11] to fit the recent data to a linear line to Eq. (5) to approximate the tangent line (as shown in Fig. 2). Every fit to determine the two parameters b and k is performed using the most recent suite of data points, enabling t_* to be calculated based on Eq. (8). For both cases of $\chi = 1$ and $\chi = 0.5$, t_* tends to converge toward the actual failure time, with a linear relation with time (Fig. 4) that commonly intersects with the straight line of $t = t_*$. Although the fluctuations induced by the noise will increase with a decrease in the number of data points used in the fit, this does not change the total linear trend. This demonstrates that this method may indeed yield an earlier and more accurate blind prediction of the failure time.

It should be mentioned that in the early stage, the fluctuations induced by noise increase with a decrease in the number of data points used in the fit. However, these do not affect the total linear trend of t_* converging to t_f. In the vicinity of t_f, an increase in the number of data points used in the fit will lead to a deviation, although this is very slight and has little effect on the total linear trend. Thus, in practical application, more data points should be used in the fit during the early stage where the gradient of the inverse rate changes only slowly,

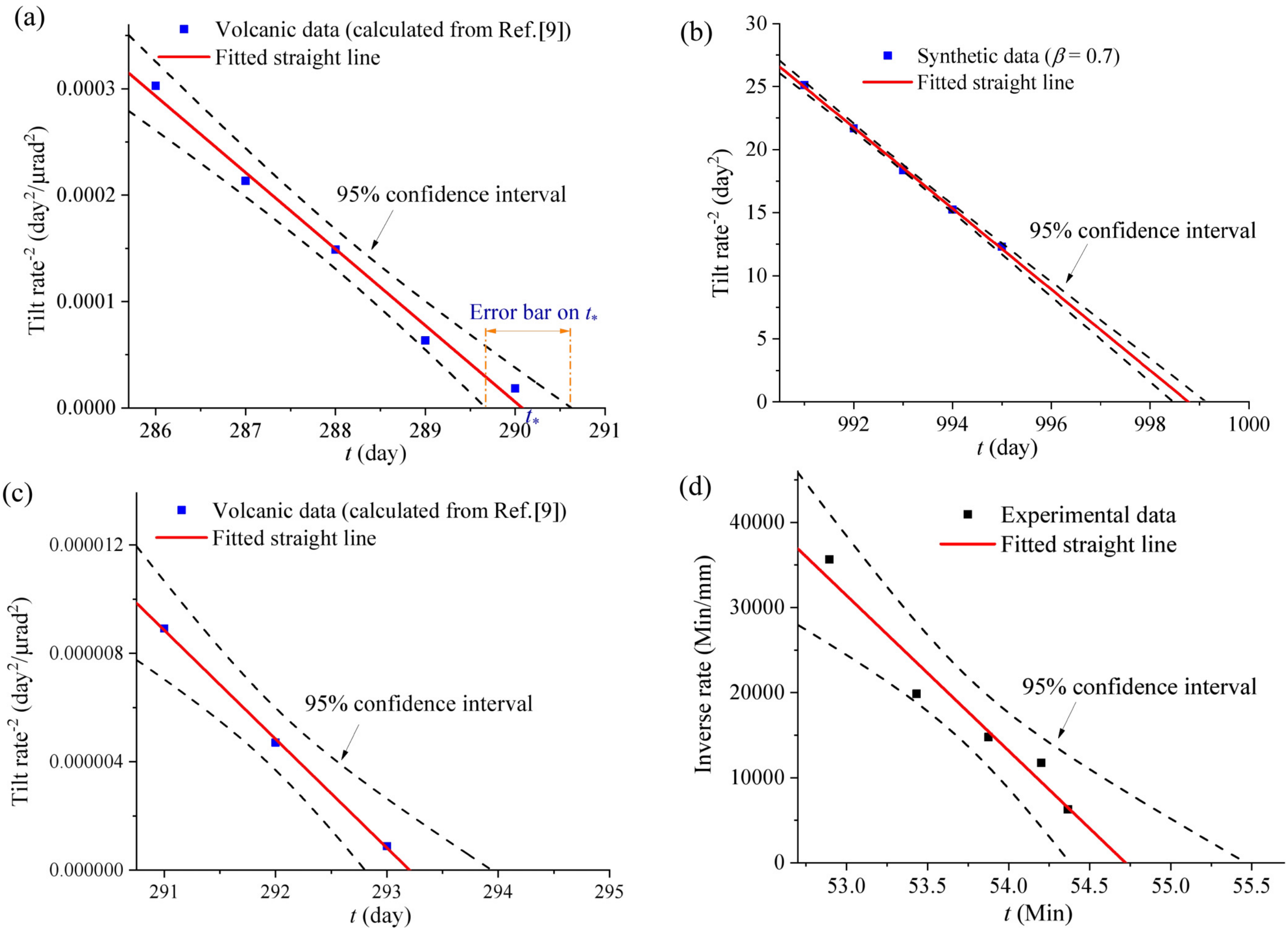

FIG. 6. Example linear estimations and error bars of t_* for real volcanic, synthetic, and real experimental data including confidence limits and the error of extrapolation to t_*. Estimation examples with (a) five real volcanic data points, (b) five synthetic data points, (c) three real volcanic data points, and (d) five real experimental data points.

then decreasing the number of data points when the gradient changes rapidly.

Now, let us evaluate this method through the use of data from laboratory creep-relaxation [35], creep [11,36], and monotonic loading experiments, and from observations of deformations (tilt data) approaching sector collapse/volcanic eruption [9]. In these examples, we calculate the values of $\dot{\Omega}^{-1}$ and $\dot{\Omega}^{-2}$ in the final stages of acceleration. The "simple moving-time" technique is used to perform a linear fit at every observable time. Clearly, the estimated values t_* of the failure times converge to the actual failure (collapse/eruption) time with a linear tendency for all three examples where the values of β are individually close to [Fig. 5(b)], less than [Fig. 5(a)] and larger than 1.0 [Fig. 5(c)]. This method presents a good prediction that is very close to the actual value for all three cases. For these volcanic eruption data [Fig. 5(c)], the three intersection points do not coincide, but they span a very short period of less than two days. This demonstrates that this method is effective in limiting the prediction to a small and diminishing range as the system progresses to failure.

V. EXPONENT VALUES IMPLYING DIFFERENT FAILURE MODES

Integration of Eq. (1) gives

$$\Omega_f - \Omega = \beta C(t_f - t)^{1-\beta}. \quad (10)$$

This indicates that $\beta > 1$ implies that the accumulation quantity Ω tends to infinity as time approaches the failure time. Thus, failure for the case where $\beta > 1$ could represent a different physical mode of failure from that of where $\beta < 1$. Double integration of Eq. (2) gives the same conclusion that Ω tends to infinity when $\alpha < 2$. Thus, $\beta = 1.0$ ($\alpha = 2$) could be a threshold magnitude implying a transition in failure modes. Conversely, when $\beta < 0.5$, Eq. (10) dictates that the inverse rate $(\mathrm{d}t/\mathrm{d}\Omega)_f = 0$ at the failure time and $(\mathrm{d}^2t/\mathrm{d}\Omega^2)_f$ each tend to infinity. As a consequence, the curve has an infinite curvature at the failure point. So, the value of $\beta < 0.5$ could represent another type of failure different from catastrophic failure—for example, creep. In laboratory creep, relaxation creep, and monotonic increase displacement catastrophic failure experiments [36] of brittle granite and marble rocks, β usually ranges from 0.5 to 1.0 [23]. For the cases of β ranging from 0.5 to 1.0, the estimated failure times t_* recovered before the catastrophic failure by assuming $\chi = 0.5$ and $\chi = 1.0$ gives the lower and upper bound of the actual failure time [Fig. 5(a)].

VI. DISCUSSION AND CONCLUSIONS

Our findings show that the estimating time to failure t_* by updating and using the most recent data points for any value of χ linearly converges to the actual failure time. This promises a robust method for the early, accurate, and blind prediction of failure time where the power-law exponent β is unknown—as is the case in all forecasts. The failure time can be determined by linearly extending the curve of t_* with respect to time to the line $t = t_*$. Alternatively, this may be determined from the intersection of two extended lines of t_* versus time, which are calculated from any two arbitrarily assumed values of χ.

The fluctuations of t_* that are induced by noise do not influence the overall tendency of the curve to linearly converge toward the actual failure time. In practical application, more data points could be used for every fit at the early stage because the gradient of the curve of $\dot{\Omega}^{-1/\chi}$ changes very slowly so that the effects of noise can be suppressed. Otherwise, the random uncertainty induced by the noise in the signal on the estimations of t_* may significantly influence the extrapolation of a linear-fit prediction of t_f. For example, in the synthetics, the ratio of the input-noise amplitude to the true signal in the data for the early phase is 10^{-3}. But this leads to significant fluctuations in the estimated t_* in this stage when the number of data points used in the fit is small (Fig. 4). Furthermore, error bars in t_* are also estimated through the method illustrated in Fig. 6. In order to compare effects of the noise levels in the synthetic and real volcanic data on estimation uncertainty, as an example, Figs. 6(a) and 6(b) plot the estimation results for five days before the eruption time using both real volcanic and synthetic data. This shows that the error bars on t_* for these two set data are of the same order and comparable. The error bars in estimated failure time t_* in Fig. 5 show that the confidence limits on the forecast failure time at early time is much larger, before then converging with time (as in Ref. [10]). It should be stated that the percentage error in the present results for synthetic data is generally less than that for the real data. In practical forecasts, there is always the potential for unconscious bias. With time approaching to the failure time, the values of rate increase rapidly and the noise has little effect on the calculated values of t_*. At this stage, we should decrease the number of data points involved in every fitting step since, in the vicinity of the actual failure time, the gradient of the curve of $\dot{\Omega}^{-1/\chi}$ changes rapidly. At this stage, the incorporation of more data points in every fitting step will result in the calculated results of t_* deviating more significantly from the linear tendency [Figs. 3(b) and 4(b)]—although this deviation is slight and does not change the total trend. Thus, in practical application, more data points should be captured within the sampling window and used in the early-stage fitting where the gradient of the inverse rate changes only slowly. The number of data points may then be decreased when the gradient changes rapidly.

In application of this method, we can first calculate $\dot{\Omega}^{-1/\chi}$ from any measurable quantity (displacements, strains, RSAM, AE) Ω for any convenient magnitude of χ. Then, a sequence of estimated failure times t_* can be calculated for every observable time by using the most recent data points. The curve of $\dot{\Omega}^{-1/\chi}$ versus time is upwardly convex for $\chi > \beta$ and concave for $\chi < \beta$. Generally, the inverse rate for $\chi = 1$ or square of inverse rate ($\chi = 0.5$) is recommended in performing the prediction. In unaxial compression tests on rocks, conducted by monotonically increasing the loadpoint displacement, the power exponent β has been found to range from 0.5 to 1.0. In this case, the estimated values of t_* based on $\chi = 1$ and $\chi = 0.5$ constrain the upper and lower bound of the failure time, respectively.

ACKNOWLEDGMENTS

This work is supported by National Natural Science Foundation of China (Grant No. 12472083) and the Key Research and Development Projects of Hebei Province (Grant No. 22375407D).

The authors declare no competing financial interests.

DATA AVAILABILITY

The data that support the findings of this article are openly available [37].

[1] B. Voight, A method for prediction of volcanic eruptions, Nature (London) **332**, 125 (1988).

[2] B. Voight, A relation to describe rate-dependent material failure, Science **243**, 200 (1989).

[3] B. Voight and R. R. Cornelius, Prospects for eruption prediction in near real-time, Nature (London) **350**, 695 (1991).

[4] C. R. J. Kilburn and D. N. Petley, Forecasting giant, catastrophic slope collapse: Lessons from Vajont, northern Italy, Geomorphology **54**, 21 (2003).

[5] C. R. J. Kilburn and B. Voight, Slow rock fracture as eruption precursor at Soufriere Hills, volcano, Montserrat, Geophys. Res. Lett. **25**, 3665 (1998).

[6] C. R. J. Kilburn, Precursory deformation and fracture before brittle rock failure and potential application to volcanic unrest, J. Geophys. Res. **117**, B02211 (2012).

[7] I. G. Main, Applicability of time-to-failure analysis to accelerated strain before earthquakes and volcanic eruptions, Geophys. J. Int. **139**, F1 (1999).

[8] S. W. Hao, C. Liu, C. S. Lu, and D. Elsworth, A relation to predict the failure of materials and potential application to volcanic eruptions and landslides, Sci. Rep. **6**, 27877 (2016).

[9] R. Cornelius and B. Voight, Graphical and PC-software analysis of volcano eruption precursors according to The Materials

Failure Forecast Method (FFM), J. Volcanol. Geotherm. Res. **64**, 295 (1995).
[10] A. F. Bell, M. Naylor, M. J. Heap, and I. G. Main, Forecasting volcanic eruptions and other material failure phenomena: An evaluation of the failure forecast method, Geophys. Res. Lett. **38**, L15304 (2011).
[11] S. W. Hao, H. Yang, and D. Elsworth, An accelerating precursor to predict "time-to-failure" in creep and volcanic eruptions, J. Volcanol. Geotherm. Res. **343**, 252 (2017).
[12] D. L. Turcotte, W. I. Newman, and R Shcherbakov, Micro and macroscopic models of rock fracture, Geophys. J. Int. **152**, 718 (2003).
[13] J. Vasseur, F. B. Wadsworth, M. J. Heap, I. G. Main, Y. Lavallée, and D. B Dingwell, Does an inter-flaw length control the accuracy of rupture forecasting in geological materials? Earth Planet. Sci. Lett. **475**, 181 (2017).
[14] M. Saito, Forecasting time of slope failure by tertiary creep, in *Proceedings of 7th International Conference on Soil Mechanics and Foundation Engineering* (Sociedad Mexicana de Mecánica de Suelos, Mexico, 1969), pp. 677–683.
[15] D. Petley, M. Bulmer, and W. Murphy, Patterns of movement in rotational and translational landslides, Geology **30**, 719 (2002).
[16] R. R. Cornelius and P. A Scott, A materials failure relation of accelerating creep as empirical description of damage accumulation, Rock Mech. Rock Eng. **26**, 233 (1993).
[17] Y. Lavallée *et al.*, Seismogenic lavas and explosive eruption forecasting, Nature (London) **453**, 507 (2008).
[18] M. J. Heap, P. Baud, P. G. Meredith, A. F. Bell, and I. G Main, Time-dependent brittle creep in Darley Dale sandstone, J. Geophys. Res. **114**, B07203 (2009).
[19] M. J. Heap, P Baud, P. G. Meredith, S. Vinciguerra, A. F. Bell, and I. G. Main, Brittle creep in basalt and its application to time-dependent volcano deformation, Earth Planet. Sci. Lett. **307**, 71 (2011).
[20] R. Smith, P. R. Sammonds, and C. R. J. Kilburn, Fracturing of volcanic systems: Experimental insights into pre–eruptive conditions, Earth Planet. Sci. Lett. **280**, 211(2009).
[21] J. Vasseur, F. B. Wadsworth, Y. Lavallée, A. F. Bell, I. G. Main, and D. B. Dingwell, Heterogeneity: The key to failure forecasting, Sci. Rep. **5**, 13259 (2015).
[22] Y. C. Wang., B. J. Zhang, and S. W Hao, Time-dependent brittle creep-relaxation failure in concrete, Mag. Concr. Res. **68**, 692 (2016).
[23] J. Xue, S. W. Hao, J. Wang, F. J. Ke, C. S. Lu, and Y. L. Bai, The changeable power law singularity and its application to prediction of catastrophic rupture in uniaxial compressive tests of geomedia, J. Geophys. Res. Solid Earth **123**, 2645 (2018).
[24] R. Cornelius and B. Voight, Seismological aspects of the 1989–1990 eruption at Redoubt Volcano, Alaska: the Materials Failure Forecast Method (FFM) with RSAM and SSAM seismic data, J. Volcanol. Geotherm. Res. **62**, 469 (1994).
[25] A. F. Bell and C. R. J. Kilburn, Precursors to dyke-fed eruptions at basaltic volcanoes: Insights from patterns of volcano-tectonic seismicity at Kilauea volcano, Hawaii, Bull. Volcanol. **74**, 325 (2012).
[26] D. N. Petley, T. D. Higuchi, J. Petley, M. H. Bulmer, and J. Carey, Development of progressive landslide failure in cohesive materials, Geology **33**, 201 (2005).
[27] C. R. J. Kilburn, Multiscale fracturing as a key to forecasting volcanic eruptions, J. Volcanol. Geotherm. Res. **125**, 271 (2003).
[28] R. Smith, C. R. J. Kilburn, and P. R. Sammonds, Rock fracture as a precursor to lava dome eruptions at Mount St Helens from June 1980 to October, 1986, Bull. Volcanol. **69**, 681 (2007).
[29] R. Smith and C. R. J. Kilburn, Forecasting eruptions after long repose intervals from accelerating rates of rock fracture: The June 1991 eruption of Mount Pinatubo, Philippines, J. Volcanol. Geotherm. Res. **191**, 129 (2010).
[30] J. Corcoran, Rate-based structural health monitoring using permanently installed sensors, Proc. R. Soc. A **473**, 20170270 (2017).
[31] A. Boué, P. Lesage, G. Cortés, B. Valette, and G. Reyes-Dávila, Real-time eruption forecasting using the material Failure Forecast Method with a Bayesian approach, J. Geophys. Res. **120**, 2143 (2015).
[32] C. Kilburn, G. De Natale, and S. Carlino, Progressive approach to eruption at Campi Flegrei caldera in southern Italy, Nat. Commun. **8**, 15312 (2017).
[33] R. Robertson and C. Kilburn, Deformation regime and long-term precursors to eruption at large calderas: Rabaul, Papua New Guinea, Earth Planet. Sci. Lett. **438**, 86 (2016).
[34] A. F. Bell, M. Naylor, and I. G. Main, The limits of predictability of volcanic eruptions from accelerating rates of earthquakes, Geophys. J. Int. **194**, 1541 (2013).
[35] S. W. Hao, B. J. Zhang, J. F. Tian, and D. Elsworth, Predicting time-to-failure in rock extrapolated from secondary creep, J. Geophys. Res. Solid Earth **119**, 1942 (2014).
[36] S. W. Hao, C. Liu, Y. C. Wang, and F. Q. Chang, Scaling law of average failure rate and steady-state rate in rocks, Pure Appl. Geophys. **174**, 2199 (2017).
[37] Zenodo repository, https://doi.org/10.5281/zenodo.15347898.